JOURNAL OF MATERIALS SCIENCE 23 (1988) 3173–3180

The effect of δ alumina fibre arrays on the age-hardening characteristics of an Al–Mg–Si alloy

C. M. FRIEND, S. D. LUXTON
Materials Technology Group, Royal Military College of Science, Shrivenham, Wiltshire, SN6 8LA, UK

The effect of δ alumina fibre arrays on the age-hardening characteristics of an Al–Mg–Si alloy (6061) has been investigated by means of hardness and electrical resistivity measurements, and optical, scanning and transmission electron microscopy. It is shown that the fibre array can have a considerable effect on the age-hardening response of the matrix alloy in metal matrix composites, causing suppression of GP zone formation which inhibits natural ageing and considerably reduces the peak hardening produced during artificial ageing. The reduced hardening potential of the composites during artificial ageing is shown to result from a competition between GP zone formation and heterogeneous nucleation of the β' intermediate precipitate on lattice defects. The most probable cause of both phenomena is shown to be lack of quenched-in vacancies following solution treatment, due to the availability of a large number of vacancy sinks at the fibre–matrix interfaces.

1. Introduction

There is considerable technological interest in Metal Matrix Composites (MMC) at the present time since materials reinforced with high-strength fibres represent a unique method for tailoring properties to suit particular applications. The use of a metal matrix also produces excellent matrix-controlled properties [1] such as high working temperatures, improved electrical/thermal conductivity and high shear and off axis strengths. However, most work on fibre-reinforced MMC has concentrated on optimization of the composite properties by changing the type of fibre and its size and orientation. Whilst this is very important, little consideration has been given to the properties of the matrix and how they contribute to the final properties of the composite.

The matrix contributes several important properties. It allows the composite to be efficiently bonded, provides the fibre with environmental protection and enables stresses to be internally transferred to and from the fibres. It has also been recently shown [2, 3] that in randomly oriented short-fibre reinforced composites the matrix properties play a major role in controlling the reinforcement behaviour of the composites.

Most of the alloys which have been employed as matrices in MMC are light alloys, particularly those based on aluminium. These matrix alloys have included both non-heat-treatable and heat-treatable alloys, and in the case of the latter it is now clear [4] that the matrices constitute a metallurgically "active" component of the MMC whose properties can be deliberately altered to influence the properties of the final composite. It is usually assumed, however, that these matrix alloys heat-treat in a manner identical to that of the unreinforced alloy. Little consideration is, therefore, given to the possible effects of the fibre array on the structure of the heat-treated matrix and its resulting properties.

There is little published data describing the age-hardening response of alloys containing fibre arrays. Although Rack [5] has shown that the presence of SiC whiskers can considerably influence the age hardening of aluminium alloy 6061, the most extensive evidence for the effect of a fine dispersed second phase on age hardening is the work of Ceresara and Fiorini [6, 7] on Sintered Aluminium Powder (SAP) alloys. From hardness and resistivity measurements on Al–Mg–Si/Al_2O_3 and Al–Cu/Al_2O_3, Ceresara and Fiorini observed that an oxide content of approximately 3% was sufficient to inhibit G.P. zone formation and natural ageing. During artificial ageing these SAP alloys also prematurely over-aged resulting in reduced age hardening compared to the conventional powder materials. Thus in SAP the age hardening behaviour of heat-treatable alloys was considerably altered by the presence of small alumina particles. The work of both Rack [5] and Ceresara and Fiorini [6, 7] therefore implies that the heat-treatment response of an alloy containing fine ceramic fibres should be significantly different from that of the unreinforced alloy. The present work was, therefore, undertaken to discover whether fibre arrays have such an effect on the precipitation hardening response of fibre-reinforced MMC.

2. Experimental procedures

The composites employed in this investigation were based on a heat-treatable aluminium alloy matrix reinforced with short alumina fibres. The matrix alloy employed was 6061 (Al–1% Mg–0.6% Si–0.5% Cu–0.2% Cr) and the reinforcement was "Saffil" (ICI trademark) which is basically a δ-Al_2O_3 fibre containing a small proportion of silica.

0022–2461/88 $03.00 + .12

The composites were manufactured by the pressure infiltration route [8] using preforms with nominal fibre volume fractions (V_f) of 0.05 and 0.25. The preforms were preheated to 350° C and infiltrated with aluminium alloy superheated to 1000° C using a pressure of 25 MPa applied for one minute. Excess alloy was used in order to obtain a sample of unreinforced matrix alloy cast under identical conditions to those employed for the composite. When the casting reached room temperature the composite and squeeze cast alloy were separated producing discs of composite and alloy. Specimens were machined from both discs for testing and microscopy.

2.1. Heat-treatment

All specimens were heat-treated in two stages:

(i) solution-treated at 529° C for 1 h, followed by water quenching, and

(ii) aged either isochronally or isothermally.

The hardness and resistivity of the materials were measured following solution treatment and the microstructure characterized by microscopy. The specimens were then isochronally or isothermally aged. Specimens were isochronally aged for 30 min at temperatures between 20 and 300° C. From the results of this isochronal ageing an artificial ageing temperature of 140° C was then selected for isothermal ageing. Specimens were also naturally aged at 20° C. The hardness and resistivity of the specimens were measured following isochronal ageing and these properties were monitored during isothermal ageing. The microstructures of the aged specimens were also investigated by optical, transmission (TEM) and scanning electron (SEM) microscopy.

2.2. Resistivity measurements

Resistivity measurements were carried out by a four-probe d.c. technique. A direct current of one amp was passed through a specimen 75 mm long and 4 mm diameter, and the voltage drop between the inner two probes measured using a high impedance digital voltmeter (DVM), accurate to $\pm 1\,\mu$V. The resistance of the specimen was calculated from this potential drop using Ohm's law, and the dimensionally independent resistivity calculated from this resistance using the equation:

$$\varrho = RA/L$$

where ϱ is the resistivity of the material, R the specimen resistance, A the cross-sectional area of the specimen and L the inner probe separation.

Since measurements of this type are temperature dependent, they were conducted at 20 ± 1° C to avoid errors due to fluctuations in the ambient temperature. The resistivity change during ageing was characterized by the parameter $\Delta\varrho$ which was calculated in the following way

$$\Delta\varrho = \varrho(\text{aged}) - \varrho(\text{sol})$$

where ϱ(aged) and ϱ(sol) are the aged and solution-treated resistivities respectively.

2.3. Hardness measurements

The macroscopic hardness of the alloy and composites was characterized by Vickers hardness, measured with a 10 kg load. The microhardness of the alloy and composite matrices were also measured in the peak-aged condition using a Vickers microhardness indenter fitted to a metallurgical microscope. The load employed in these measurements was 100 g.

2.4. Microscopy

Microscopy was carried out using optical, transmission (TEM) and scanning electron (SEM) microscopes. Optical microscopy was conducted to assess any microstructural differences between the unreinforced alloy and composites in the various heat-treated conditions, and to identify the volume fraction of reinforcement in the fabricated composites. The volume fraction of reinforcement was determined by a point count analysis.

SEM was employed to characterize the preforms prior to infiltration and TEM was performed on the unreinforced alloy and composites in the peak-hardened condition to establish the nature and morphology of the age-hardening precipitates. TEM specimens of the unreinforced alloy were electrochemically thinned, however this was impossible for the composites because of differential electro-polishing effects. The composite materials were therefore ion-beam thined.

3. Results

3.1. Optical and scanning electron microscopy

Fig. 1 shows a SEM micrograph of a nominally 0.25 V_f preform which clearly shows the pseudorandom nature of the fibre orientation in these preforms and composites. Fig. 2 shows optical micrographs of the nominally 0.05 and 0.25 V_f composites in the cast condition. Both composites were of good quality with an even distribution of fibre throughout the matrix and there was no evidence of porosity or the ingress of dross. Quantitative microscopy revealed that the composite of nominal 0.05 V_f had a true fibre fraction of 0.08, and the nominally 0.25 V_f a volume fraction of 0.26. Fig. 3 shows optical micrographs of the unreinforced alloy and a 0.26 V_f composite in the solution-treated condition. In both cases solution-treatment fully dissolved the intragranular precipitates of Mg_2Si,

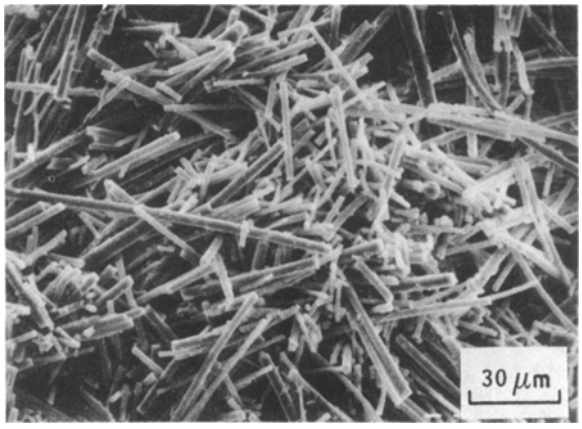

Figure 1 SEM micrograph of an uninfiltrated 0.26 V_f preform.

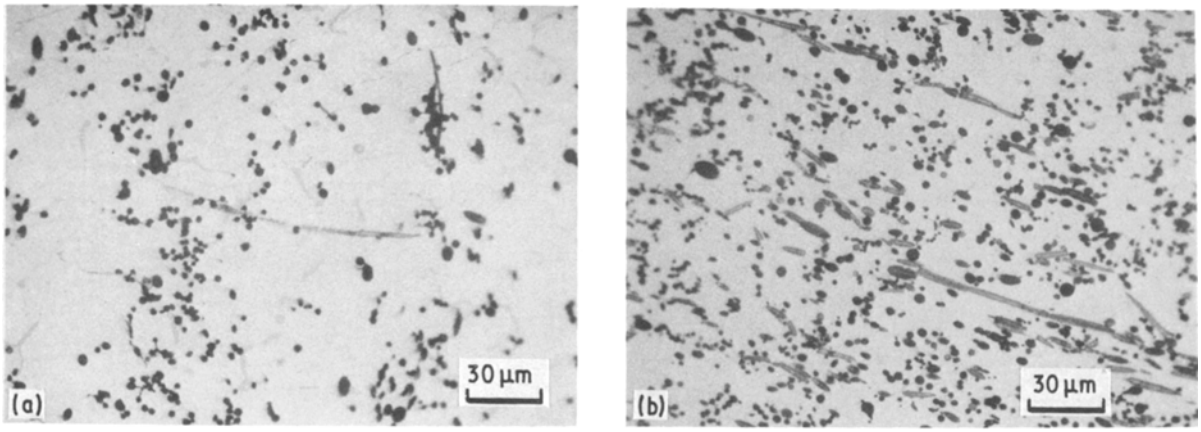

Figure 2 Optical micrographs of (a) 0.08 V_f and (b) 0.26 V_f composites in the as-cast condition.

leaving only the script-like intermetallic compound $Fe_3Al_{12}Si$ which was insoluble during normal age-hardening treatments.

3.2. Isochronal ageing

Fig. 4 shows the hardness change during ageing of the unreinforced alloy, and 0.08 and 0.26 V_f composites. Both composites exhibited a behaviour which deviated from that of the unreinforced alloy, with the magnitude of the deviation dependent on the volume fraction of reinforcement. The solution-treated hardness of the 0.26 V_f composite was significantly higher than that of the unreinforced alloy, however on ageing it hardened by only a small amount (less than 25% of the hardness change observed in the unreinforced alloy). The result of this was a significantly lower peak hardness. The behaviour of the 0.08 V_f composite deviated only slightly from the unreinforced alloy response, having a similar solution-treated hardness and hardening to a lesser degree than the unreinforced alloy. The 0.08 V_f composite therefore exhibited ageing characteristics which were intermediate between the unreinforced alloy and 0.26 V_f composite.

The different ageing responses of these composites can also be seen from the resistivity results. Table 1 contains the solution-treated resistivities of the unreinforced alloy and composites and Fig. 5 shows the change in resistivity ($\Delta\varrho$) following isochronal ageing. The resistivity change during ageing of the unreinforced alloy exhibited an initial increase in resistivity following low temperature ageing (0–100° C) and a decrease in resistivity at higher temperatures (150–300° C). The composite behaviour following similar ageing deviated from this response, most markedly in the higher volume fraction composite. The 0.26 V_f composite exhibited no change in resistivity until approximately 150° C. At temperatures above 150° C there was then a decrease in resistivity. The resistivity change of the 0.08 V_f composite showed an intermediate response with an initial increase in resistivity at low temperatures. However the magnitude of this increase was smaller than that observed in the unreinforced alloy.

3.3. Natural ageing

Fig. 6 shows the natural age-hardening characteristics of the unreinforced alloy and a 0.26 V_f composite. The main feature of this ageing was the hardening observed in the unreinforced alloy, and its complete absence in the composite even after 10^5 min. Fig. 7 shows the resistivity changes associated with this natural ageing. The resistivity of the unreinforced alloy showed a characteristic increase on ageing whereas the 0.26 V_f composite exhibited a small decrease. Both trends were continuing at 10^5 min.

3.4. Isothermal artificial ageing

The resistivity and hardness changes of the unreinforced alloy and 0.26 V_f composite during isothermal

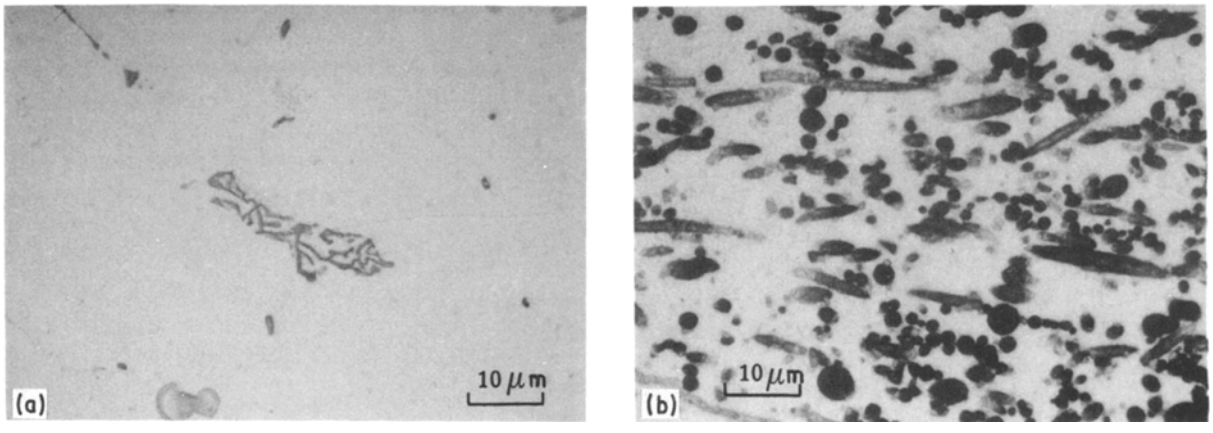

Figure 3 Optical micrographs of (a) unreinforced alloy and (b) 0.26 V_f composite in the solution-treated condition (etch 3% HF).

TABLE I Average solution-treated resistivities of the unreinforced alloy and composites

Material	$\varrho_{(SOL)}$ (nΩm)
Unreinforced alloy	43.6
0.08 V_f composite	47.9
0.26 V_f composite	60.8

TABLE II Average micro and macro peak-hardnesses of the unreinforced alloy and composite matrices

V_f	Micro-hardness	Macro-hardness
0	120	120
0.8	104	–
0.26	75	–

ageing at 140° C are shown in Figs 8 and 9. The characteristic increase in resistivity was present in the unreinforced alloy (Fig. 8) during the early stages of ageing, but was absent in the 0.26 V_f composite. The composite exhibited no change in resistivity at shorter ageing times and then a decrease in resistivity after more extensive ageing. Both the unreinforced alloy and 0.26 V_f composite hardened (Fig. 9), however the onset of hardening was delayed in the composite and the level of hardening was significantly lower than that obtained from the unreinforced alloy.

3.5. Matrix hardness

The significantly different response of the composite matrices to age hardening can be seen from Table II. The microhardness of the matrix at peak hardness (aged 30 min at 200° C) decreased with increasing volume fraction of fibre reinforcement.

3.6. Transmission electron microscopy

Fig. 10 shows the microstructure of the unreinforced alloy in the peak-aged condition, with dislocation lines and tangles clearly visible but with no visible precipitation. At higher magnification a fine precipitate was just resolvable but these precipitates were close to the resolution limits of the instrument. Fig. 11 shows the microstructure of a 0.26 V_f composite following an identical heat treatment. The microstructure of the matrix alloy contained coarse β'-Mg_2Si precipitation in a Widmanstatten morphology. Dislocation density differences between the unreinforced alloy and composites were difficult to assess since the dislocations were in the form of long lines in the unreinforced alloy, but consisted of short dislocation lines in the composites. Qualitative assessment however indicated that there was little difference in overall dislocation density.

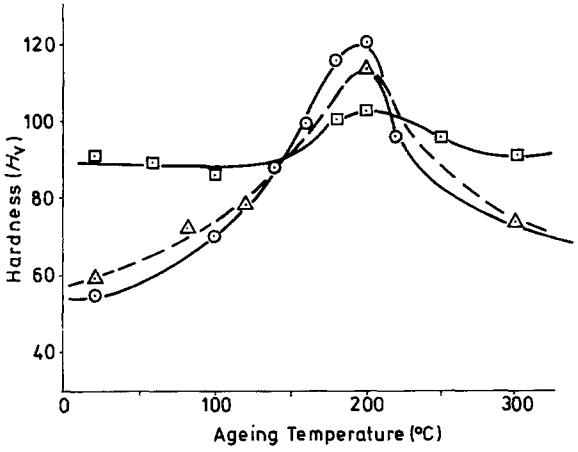

Figure 4 Isochronal age-hardening characteristics of the unreinforced alloy (○), and 0.08 (△) and 0.26 (□) V_f composites.

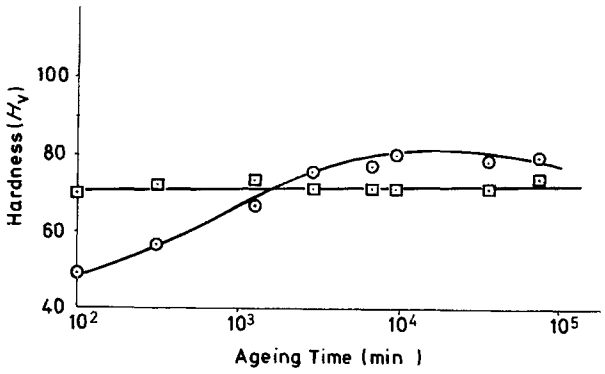

Figure 6 Natural age-hardening characteristics of the unreinforced alloy (○) and 0.26 (□) V_f composite.

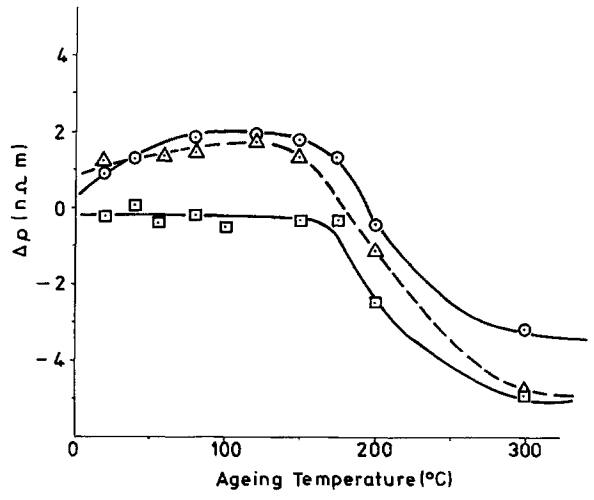

Figure 5 Resistivity changes following isochronal ageing of the unreinforced alloy (○) and 0.08 (△) and 0.26 (□) V_f composites.

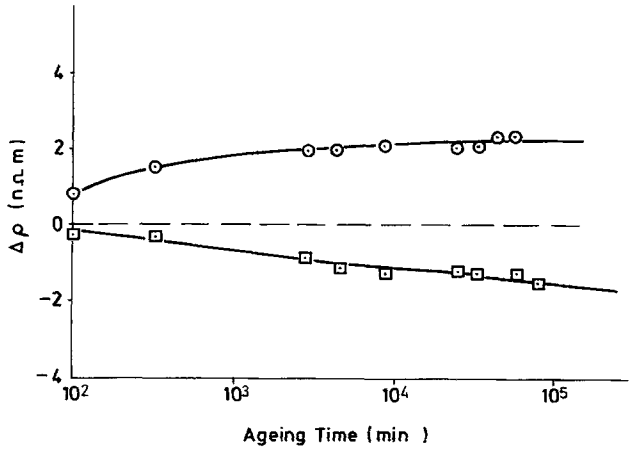

Figure 7 Resistivity change of the unreinforced alloy (○) and 0.26 (□) V_f composite during natural ageing.

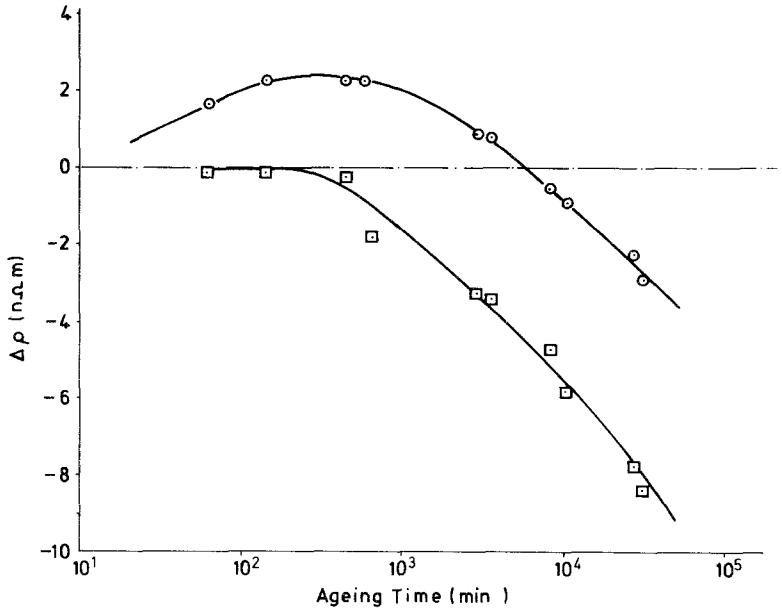

Figure 8 Resistivity change of the unreinforced alloy (○) and 0.26 V_f composite (□) during artificial ageing at 140° C.

4. Discussion

The data presented above clearly shows that the presence of a δ-Al_2O_3 fibre array has a significant effect on the age-hardening characteristics of aluminium alloy 6061. This is illustrated in Table II which shows that as the volume fraction of reinforcement increases the peak hardness attainable from the matrix decreases. It must, therefore, be this phenomenon which results in the smaller overall ageing potential of the composites (Fig. 4).

The detailed age-hardening response of this type of aluminium alloy, and the effect of fibre arrays on its response can be investigated most easily by considering a combination of both mechanical property (e.g. hardness) and resistivity changes during ageing. Typical data of this type is shown in Fig. 12 for the isochronal ageing of the unreinforced alloy. A cross-plot of this type can be used to identify the individual stages of age hardening. It is clear that there are three distinct stages in the ageing of 6061. At lower temperatures (Stage I, $T < 115°$ C) there is an increase in resistivity accompanied by a small increase in hardness. At higher ageing temperatures (Stage II, $115 < T < 200°$ C) the resistivity decreases and is accompanied by a rapid increase in the rate of hardening. At still higher temperatures (Stage III, $T > 200°$ C) this decrease in resistivity becomes associated with a decrease in hardness. The intermediate stages in the age-hardening of 6061 are now well established [9] and it is clear that Stages I and III coincide with the three documented stages of precipitation hardening. Stage I therefore represents the formation of G.P. zones which result in a small increase in resistivity and a slight increase in hardness [10], Stage II the formation of β'-Mg_2Si, the intermediate precipitate and Stage III with over-ageing and Ostwald ripening of the equilibrium precipitates of β-Mg_2Si. A simple cross-plot of this type, accompanied by knowledge of the precipitation sequence during ageing, can, therefore, be used to fully characterize the ageing response of this alloy. This technique will therefore be used to analyze the effect of the fibre array on the age-hardening response of the matrix in these MMC.

The cause of the reduction in age-hardening potential in MMC matrices can be identifed by cross-plotting the hardness and resistivity changes of the composites during ageing. There is a potential problem however, since the composite hardness contains contributions from both the metallurgically active matrix and the fibres. This is easily resolved if it is assumed that the age-hardening treatment only affects the matrix properties. Assuming that the composite hardness is

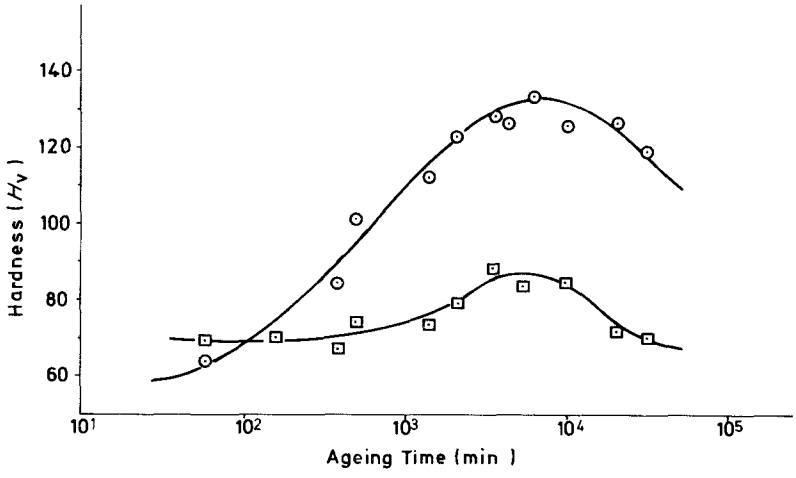

Figure 9 Age-hardening characteristics of the unreinforced alloy (○) and 0.26 V_f composite (□) during artificial ageing at 140° C.

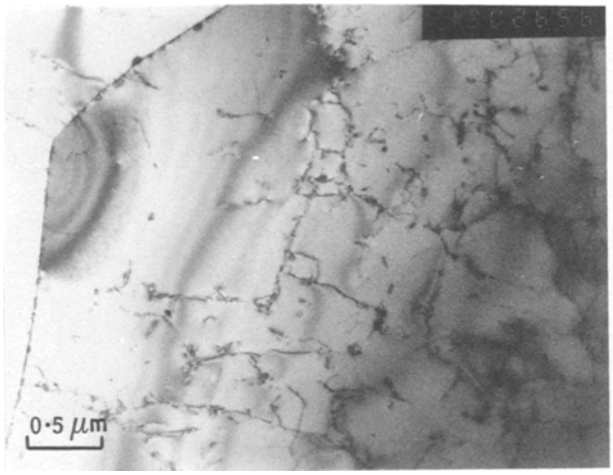

Figure 10 TEM micrograph of the unreinforced alloy in the peak-aged condition.

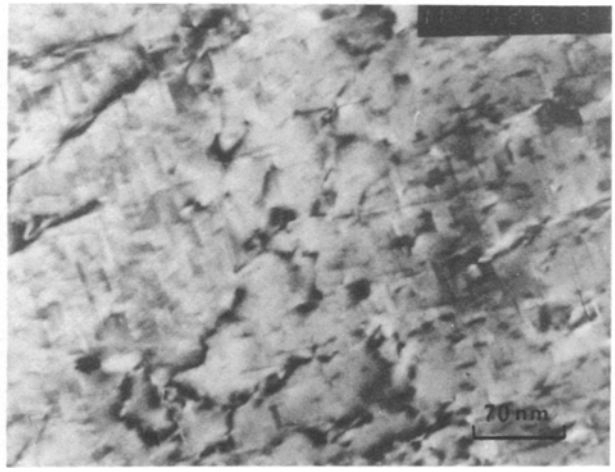

Figure 11 TEM micrograph of the matrix of a peak-aged 0.26 V_f composite.

related to the hardness of the fibres and matrix by a "modified rule of mixtures" relationship, the hardness *change* of a composite should then be related to the hardness *change* of its matrix by a simple factor equal to the matrix volume fraction, V_m. Thus the *change* in composite hardness can be used as a measure of the *change* in matrix hardness. A similar approach can also be employed for the composite resistivity changes. The result of a cross-plot of this type is shown in Fig. 13 for a 0.26 V_f composite. This shows that

(a) Stage I is absent in the 0.26 V_f composite.

(b) The peak-hardening associated with Stage II is much smaller in the composite than expected from a simple consideration of the matrix volume fraction. From Figs 4 and 5 it is also clear that these two phenomena are volume-fraction dependent. Since Stage I is suppressed it can be concluded that these alumina fibre arrays have a considerable effect on GP zone formation. This observation is supported by the cross-plotted natural-ageing data in Fig. 14. It is clear that the unreinforced alloy exhibits GP zone formation with the characteristic increase in resistivity and some age-hardening, however in the 0.26 V_f composite the fibre array causes inhibition of GP zone formation in the matrix, suppressing the increases in both resistivity and hardness. The magnitude of this effect is also volume-fraction dependent, increasing with higher reinforcement volume fractions.

The development of significant levels of hardness in this alloy is associated with the formation of β'-Mg_2Si. The level of age hardening must, therefore, depend on the size and spacing of the precipitates, which is controlled by the nature of the β' nuclei and their temperature of formation. The lack of hardening in the matrices of the composites can therefore be attributed to the formation of fewer, and coarser β' precipitates. This is consistent with the TEM micrograph in Fig. 11. The sequence of formation of the Widmanstatten morphology in the composites can be seen from the isothermal artificial ageing data cross-plotted in Fig. 15. It is clear that GP zone formation is inhibited in the composite even at elevated temperatures and Stage II modified with a lower peak-hardness and no increase in resistivity prior to β' formation. The inhibition of natural ageing and the modification of the β' morphology at higher temperatures and longer ageing times must therefore result from the inhibition of GP zone formation.

This inhibition of GP zone formation and its effect on age hardening is similar to observations in SAP

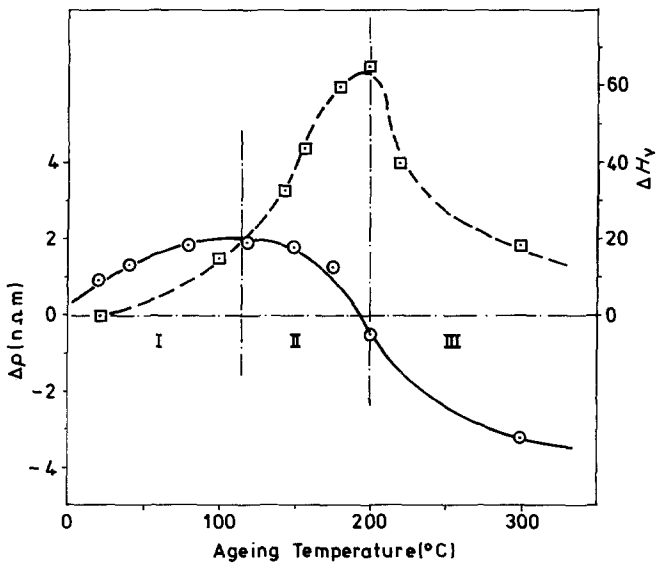

Figure 12 Cross-plot of the hardness (□) and resistivity (○) changes following isochronal ageing of the unreinforced alloy.

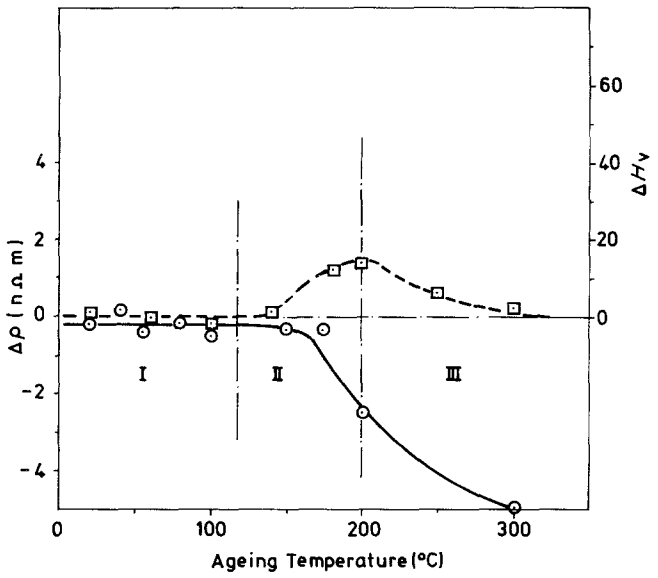

Figure 13 Cross-plot of the hardness (□) and resistivity (○) changes following isochronal ageing of a 0.26 V_f composite.

alloys [6, 7] where effects of this type have been identified which were also volume fraction dependent. In SAP alloys these phenomena have been attributed to a lack of quenched-in vacancies which were soaked up by the grain boundaries in the fine-grained matrix, and by the Al/Al_2O_3-particle interfaces. The observations in the present work suggest that a similar mechanism is responsible for the inhibition of GP zone formation in MMC matrices.

It is now well established that the formation of GP zones relies on the presence of quenched-in vacancies [11] to aid the diffusion of the Si and Mg atoms [12–14]. The inhibition of GP zone formation therefore implies that the quenched-in vacancy concentration is lower in these composites than in the unreinforced alloy, and that the concentration *decreases* with increasing fibre volume fraction. There are a number of sources for this low quenched-in vacancy concentration. The vacancies could be soaked up by

(i) α-phase grain boundaries
(ii) matrix dislocations
(iii) fibre–matrix interfaces.

The first of these vacancy sinks can be ruled out for these MMC since there was no significant difference between the grain sizes of the unreinforced alloy and composites. This implies a constant grain-boundary "vacancy-sink" potential for both the alloy and composites. Matrix dislocations could act as a source of vacancy sinks, however, as shown above there was no significant difference in dislocation density between the composite and unreinforced alloy, implying that dislocations were not the source of the inhibition of GP zone formation in the composites. Thus the fibre–matrix interfaces must play the predominant role as vacancy sinks. This is consistent with the fibre volume-fraction dependence of GP zone suppression.

The lack of GP zones not only inhibits natural ageing, but also has a considerable effect on the later stages of age-hardening. The suppression of GP zone formation at low temperatures or during the early stages of artificial ageing means that no nuclei are produced for β' formation until considerably later stages of the ageing process. This has a number of effects. Firstly β' precipitation must be supported solely by the equilibrium thermal vacancy concentration, and secondly there are no fine nuclei to enable the immediate formation of β' in a morphology which will cause significant hardening. In Al–Mg–Si alloys the GP solvus lies above the normal ageing tempertures [9] which implies that the formation of GP zones can occur at higher isochronal ageing temperatures or during the later stages of isothermal ageing. However, the formation of GP zones at these temperatures and their subsequent growth to β' will be hampered by

(i) a reduced nucleation rate, thus producing a coarser β^1 morphology and

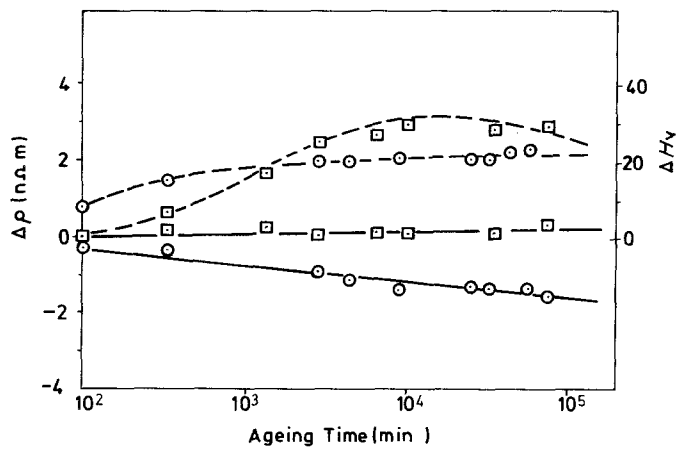

Figure 14 Cross-plot of the hardness (□) and resistivity (○) changes for the unreinforced alloy (– – –) and 0.26 V_f composite (——) during natural ageing.

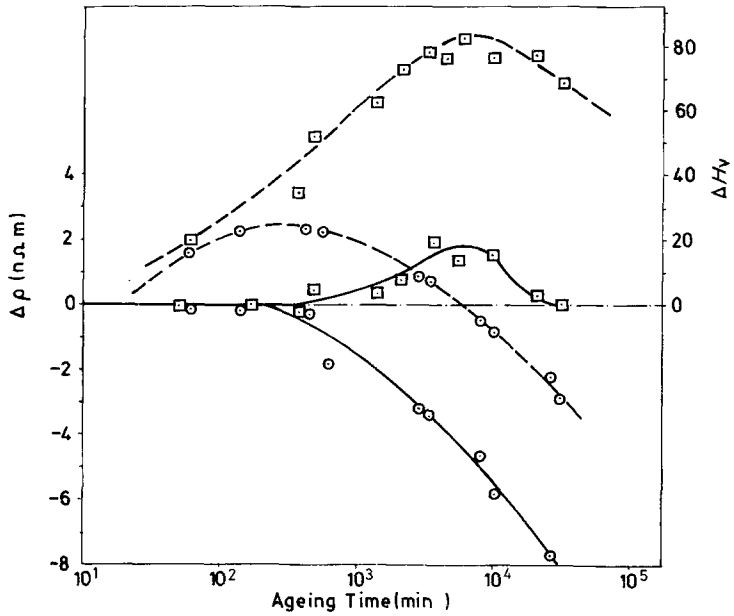

Figure 15 Cross-plot of the hardness (□) and resistivity (○) changes for the unreinforced alloy (– – –) and 0.26 V_f composite (——) during artificial ageing at 140° C.

(ii) competition from heterogeneous nucleation on dislocations.

It is clear from the data in Figs 13 and 15 and from the micrographs in Figs 10 and 11 that this latter process becomes the dominant one, aided by thermal activation and the equilibrium thermal vacancy concentration. This heterogeneous nucleation and the coarse Widmanstatten morphology results in a lower peak hardness during ageing, the magnitude depending on the volume-fraction of fibre reinforcement and thus the number of available vacancy sinks.

5. Conclusions

The age-hardening characteristics of Al-alloy 6061 are considerably altered by the presence of a δ-alumina fibre array. Fibre arrays inhibit natural ageing due to the suppression of GP zone formation, with the degree of suppression increasing with fibre volume fraction. Composites can be precipitation hardened by artificial ageing but the level of hardening is significantly lower than in the unreinforced alloy, with the level decreasing with increasing fibre volume fraction.

The most probable cause of both phenomena is the lack of quenched-in vacancies following solution treatment due to the availability of large numbers of vacancy sinks at the fibre–matrix interfaces. This lack of quenched-in vacancies inhibits GP zone formation and natural ageing, and means that artificial ageing is supported solely by the equilibrium thermal vacancy concentration. This results in a competition during artificial ageing between GP zone formation and heterogeneous nucleation of β' precipitates on lattice defects. In these composites the latter becomes the dominant process resulting in impaired hardening.

Acknowledgements

The authors acknowledge J. Bradfield, J. Crocker and A. Edwards for experimental assistance, and J. Dinwoodie (ICI Mond Division) and Docent R. Warren for the supply of Saffil preforms.

References

1. M. R. PIGGOT, "Load Bearing Fibre Composites" 1st edn (Pergamon, Oxford, 1980) p. 187–188.
2. C. M. FRIEND, *J. Mater. Sci.* **22** (1987) 3005–10.
3. *Idem*, in "Proc. 6th Int. Conf. on Comp. Mat. (ICCMVI), Imperial College, London, July 1987." Vol. 2 edited by F. L. Matthews, N. C. R. Buskell, J. Hodgkinson and J. Morton (Elsevier Applied Science, Amsterdam, 1987) p. 402.
4. J. ENGLAND and I. W. HALLS, *Scripta Metall.* **20** (1986) 697–700.
5. H. J. RACK, in "Proc. 6th Int. Conf. on Comp. Mat. (ICCMVI), Imperial College, London, July" Vol. 2 edited by F. L. Matthews, N. C. R. Buskell, J. Hodgkinson and J. Morton (Elsevier Applied Science, Amsterdam, 1987) p. 382.
6. S. CERESERA and P. FIORINI, *Powder Metall.* **1** (1979) 1–5.
7. S. CERESARA and P. FIORINI, *Powder Metall.* **4** (1981) 210–213.
8. T. W. CLYNE, M. G. BADER, G. R. CAPPELMAN and P. A. HUBERT, *J. Mater. Sci.* **20** (1985) 85.
9. I. J. POLMEAR, "Metallurgy of Light Metals" 1st. edn (Edward Arnold, London, 1981) p. 15–21.
10. R. E. SMALLMAN, "Modern Physical Metallurgy" 3rd edn (Butterworth, London, 1970) p. 423–429.
11. C. ZENER, "Proc. Int. Conf. on the Physics of Metals, Amsterdam, 1948.
12. W. DESORBO, H. N. TREAFTIS and D. TURNBULL, *Acta. Metall.* **6** (1958) 401.
13. A. KELLY and R. B. NICHOLSON, *Prog. Mater. Sci.* **10** (1963) 173.
14. E. W. HART, *Acta. Metall.* **6** (1958) 553.

Received 6 August
and accepted 22 October 1987